PNAS RESEARCH ARTICLE | EARTH, ATMOSPHERIC, AND PLANETARY SCIENCES

Tracing sources of atmospheric methane using clumped isotopes

Mojhgan A. Haghnegahdar[a,b,c,1], Jiayang Sun[a], Nicole Hultquist[a], Nora D. Hamovit[d], Nami Kitchen[e], John Eiler[e], Shuhei Ono[f], Stephanie A. Yarwood[d], Alan J. Kaufman[a,b], Russell R. Dickerson[g], Amaury Bouyon[a], Cédric Magen[a], and James Farquhar[a,b]

Edited by William D. Leavitt, Dartmouth College Department of Earth Sciences, Hanover, NH; received April 6, 2023; accepted October 5, 2023 by Editorial Board Member Amy C. Rosenzweig

We apply a recently developed measurement technique for methane (CH_4) isotopologues* (isotopic variants of CH_4—$^{13}CH_4$, $^{12}CH_3D$, $^{13}CH_3D$, and $^{12}CH_2D_2$) to identify contributions to the atmospheric burden from fossil fuel and microbial sources. The aim of this study is to constrain factors that ultimately control the concentration of this potent greenhouse gas on global, regional, and local levels. While predictions of atmospheric methane isotopologues have been modeled, we present direct measurements that point to a different atmospheric methane composition and to a microbial flux with less clumping (greater deficits relative to stochastic) in both $^{13}CH_3D$ and $^{12}CH_2D_2$ than had been previously assigned. These differences make atmospheric isotopologue data sufficiently sensitive to variations in microbial to fossil fuel fluxes to distinguish between emissions scenarios such as those generated by different versions of EDGAR (the Emissions Database for Global Atmospheric Research), even when existing constraints on the atmospheric CH_4 concentration profile as well as traditional isotopes are kept constant.

atmospheric methane | methane sources | greenhouse gas emissions | methane isotopic composition and isotopologues | methane trends

Significance

With an approximately ten-year lifetime and strong infrared absorption, methane is one of the most important greenhouse gases and a target for mitigation. Here, we describe unique measurements of rare isotopic variants of methane (isotopologues, in particular, $^{13}CH_3D$ and $^{12}CH_2D_2$) in air, which when used in combination with traditional isotope and concentration constraints, add valuable new information about the balance of atmospheric CH_4 sources. Importantly, information from these isotopologue analyses distinguishes between different proposed histories of fossil fuel to microbial methane emissions, even when the traditional isotope and concentration records are the same. Consideration of these isotopologues also supports recent assertions that increases in microbial emissions are driving the most recent rise in atmospheric methane.

Methane (CH_4) is the second most important anthropogenic greenhouse gas in Earth's atmosphere with its residence time controlled primarily by loss to reaction with the $^{\bullet}OH$ radical, and to a lesser extent by reaction with $Cl^{\bullet}$ and $O(^1D)$ as well as oxidation in soils (1). These reactions result in a lifetime of ~10 y, meaning that >98% of the methane in the atmosphere was emitted in the past 40 years. The classification as a short-lived climate pollutant also means that increases in emission rates have thus supported an increase of >15% in its globally averaged atmospheric concentration over the same period (2).

Methane is a primary target to address climate change, in large part because of its short lifetime (and potential as a greenhouse gas), which translates to changes we make today will impact what most of us witness in our lifetimes (1). It has also been highlighted that methane mitigation may be one of our best opportunities to meet targets such as those outlined in the Paris Agreement (3, 4). A complicating factor in mitigating methane is uncertainty in its global budget, especially in sources, illustrated by disagreement between bottom–up vs. top–down models (5); existing observations can be explained by different hypotheses relating changes in source fluxes, source compositions, and/or sink reactions [c.f. (6–11)]. A need therefore exists for the development of additional independent observations that can be used to increase the number of constraints controlling the processes that govern the rapid rise of methane in the atmosphere.

The rise in atmospheric methane from preindustrial levels of ~700 ppb (5) to ~1,900 ppb (2) in 2023, has not been monotonic. The buildup accelerated through most of the 20th century, only to taper off in the 1990's and then notably to stall between 1999 and 2006 (11); the early 21st century plateau was hypothesized to reflect the stabilization of sources due to a decrease in anthropogenic emissions (12). In 2007, methane resumed its rapid upward trajectory (~8–10 ppb/y) indicating renewed strengthening of CH_4 sources, a weakening of its sinks, or both (6, 11).

One approach used to improve our understanding of these temporal variations in atmospheric methane concentration has been to study isotopic forms of CH_4 such as the $^{13}CH_4$ **isotopologue** (**isotopic variant** described by bulk $\delta^{13}C$ composition†—also see *SI Appendix*) (6–11). Biogenic sources tend to release less $^{13}CH_4$ relative to $^{12}CH_4$ compared to fossil

*Bold was used wherever the definition was given for a term that for the first time appeared in the manuscript and could be considered Jargon.

†The δ notation describes the enrichment (positive values) or depletion (negative values) in parts per thousand of a rare isotope or isotopologue relative to the major isotope or isotopologue, e.g., $\delta^{13}C\,(\text{in}\,‰) = 1000 \times (((^{13}C/^{12}C)_{sample} - (^{13}C/^{12}C)_{reference})/(^{13}C/^{12}C)_{reference})$.

The authors declare no competing interest.

This article is a PNAS Direct Submission. W.D.L. is a guest editor invited by the Editorial Board.

[1]To whom correspondence may be addressed. Email: mojhganh@umd.edu.

This article contains supporting information online at https://www.pnas.org/lookup/suppl/doi:10.1073/pnas.2305574120/-/DCSupplemental.

Published November 13, 2023.

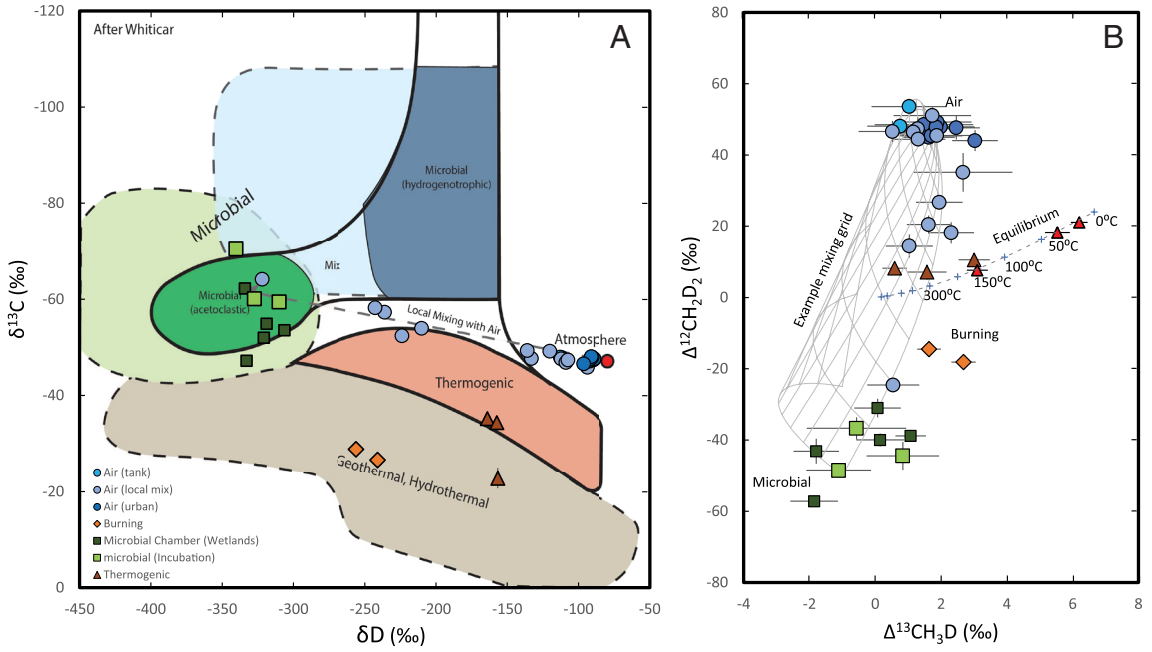

Fig. 1. (*A*) Plot of $\delta^{13}C$ and δD (‰) of methane samples measured in this study (air—blue circles; microbial wetland related—green squares; natural gas—brown triangles; biomass burning—orange diamonds) overlain on the fields of Whiticar (24). Dashed gray line shows possible trajectory for mixing of tropospheric air with local sources having microbial signatures. The red circle in Panel *A* is the composition of atmospheric methane given by ref. 22. (*B*) Plot of $\Delta^{12}CH_2D_2$ vs. $\Delta^{13}CH_3D$ (‰) illustrating the uniquely positive $\Delta^{12}CH_2D_2$ of air samples relative to the equilibrium curve (stippled gray curve labeled with temperatures from 0 to 330 °C) and samples equilibrated using with γ-alumina at 15 °C, 32 °C, and 150 °C (red triangles) following ref. 25. Data for natural gas samples (brown triangles), (biomass) burning (orange diamonds), microbial methane (light green squares are incubations; darker green squares are chamber collections). A mixing net with end members broadly matching air mixed with microbial methane is plotted in dashed gray. Mixing of air with local sources such as air from wetlands (*SI Appendix*) is hypothesized to account for the variability that is seen. The global atmospheric (tropospheric) value is hypothesized to be near the cluster of air data points but could be slightly shifted since the sampling location is at ground level and within the urban dome (enhanced methane) of the Washington, DC region.

sources (i.e., lighter $\delta^{13}C$). The proportion of atmospheric $^{13}CH_4$ to $^{12}CH_4$ increased (more positive $\delta^{13}C$) in the time leading up to the $[CH_4]$ plateau between 1999 and 2006. Since that time, the $\delta^{13}C$ has shifted to more negative values, even as the rise in concentration resumed (compare *SI Appendix*, Figs. S3 and S5*A*). Understanding what drives the fluctuations in both concentration and bulk carbon isotopic composition carries important implications for how society approaches the mitigation of this greenhouse gas—do we focus mitigation efforts on fossil sources such as natural gas leakage or on microbial sources such as landfills, agriculture, or wetlands? Other efforts have worked to use the $^{12}CH_3D$ isotopologue (variations recorded by $\delta\mathbf{D}$ compositions—see *SI Appendix*) but this record is significantly less complete (13, 14). The need for more complete records of $\delta\mathbf{D}$ as well as for other independent measures provided by the rare isotopologues of methane has been documented (13).

In this study, we explore the use of two further isotopologues of methane, the doubly substituted species $^{13}CH_3D$ and $^{12}CH_2D_2$ with variations reported as, $\Delta^{13}\mathbf{CH_3D}^{\ddagger}$ and $\Delta^{12}\mathbf{CH_2D_2}$ values as well as $\delta^{13}\mathbf{CH_3D}$ and $\delta^{12}\mathbf{CH_2D_2}$ values (ref. 14, also see *SI Appendix*). The doubly substituted isotopologues are colloquially referred to as **clumped**[§] because they have two heavy isotope substitutions and this clumping is associated with stronger bonds and makes them slightly more stable thermodynamically. Isotopes that are stochastically distributed are represented according to their relative abundance as if randomly selected from the entire population.

Interest in methane clumped isotopologues has developed over the past 15 y, insofar as they can be used 1) to document if isotopologue proportions are in equilibrium, and if so, at what temperature it was set; 2) to evaluate kinetics because these processes leave characteristic signatures between product and reactant (kinetic effects in both production and removal fractionate methane); and 3) to trace physical processes related to mixing of clumped isotopologues from specific sources into the surrounding air. All three of these processes play a part in the global atmospheric methane cycle, making the measurement of clumped isotopologues of methane a timely target for atmospheric research.

The use of clumped isotopes of methane in air has been enabled by the recent development of new instruments that can measure their ultralow abundance at high mass resolution (15–18). Also necessary were separation and purification of sufficient methane for analysis which requires processing hundreds of liters of air (described in the materials and methods and also *SI Appendix*).

Measurements of the abundance of these isotopologues are considered in the context of the global methane budget to illustrate that the information is not only independent of that provided by traditional, singly substituted isotopologues given by $\delta^{13}C$ and δD, but that this information can test hypotheses relating to the apportionment of fossil fuel and microbial sources on global, regional, and local scales. This is possible because recent studies [e.g., (19–23)] have been filling in critical information about clumped isotope compositions of various CH_4 sources and processes, the foundational information for making interpretations about methane in air.

The data presented here for singly and doubly substituted isotopologues demonstrate the applicability of this approach, which promises greater resolution of atmospheric CH_4 sources than is possible with only traditional bulk isotope techniques. We frame

[‡]The Δ notation describes the enrichment (positive values) or depletion (negative values) in parts per thousand (‰) of an isotopologue ratio relative to the stochastic ratio. For example, $\Delta^{13}CH_3D$ (in ‰) = $1000 \times ((^{13}CH_3D/^{12}CH_4)_{sample} - (^{13}CH_3D/^{12}CH_4)_{stochastic})/(^{13}CH_3D/^{12}CH_4)_{stochastic})$. In a stochastic distribution, all the stable isotopes in a given population of molecules are randomly distributed among all possible isotopologues.

[§]Gases comprised of different isotopologues are considered clumped when the $\Delta^{\#}\mathbf{X}^{\#}\mathbf{Y}$ is positive and anticlumped when $\Delta^{\#}\mathbf{X}^{\#}\mathbf{Y}$ is negative.

the information captured by various isotopic measurements using traditional isotope and isotopologue plots (Fig. 1 *A* and *B*) (see also *SI Appendix*, Table S1).

Samples

Methane was isolated from a variety of different types of samples for isotopologue measurements. Studied samples include methane extracted from near-surface air (500 to 1,000 L) collected from urban sites on and near the University of Maryland campus, from compressed air samples (commercial Airgas), and from sites located on or near the UMD campus associated with the local farm, and with wetlands. In addition to these samples, methane was extracted from smoke from a covered grill (burning wood and charcoal), from chambers deployed at the two studied wetlands, and from incubation experiments with wetland soils. Finally, methane collected from natural gas samples (Marcellus and Utica shale gas and natural gas from the UMD Chemistry Bldg) was analyzed. Additional details about the sampling locations, collection procedures, and calibration are presented in Supporting Information.

Using Isotopologue Data to Track Local Source Contributions and Mixing. In Fig. 1*A*, the traditional isotopic compositions of various sources are illustrated as colored fields (23); also on this panel is the much more narrowly defined and distinct composition for atmospheric methane (red circle). Data collected in this study largely falls within the defined fields, and data collected for ambient air (blue circles) extends from composition defined for air by ref. 24 along an array that extends towards microbial sources. Air samples were all collected in the planetary boundary layer within 3 m of ground level. Those showing mixing (meaning the influence of local sources) were generally collected in the early morning around sunrise near sites of methane emission and contained methane that accumulated overnight due to low nocturnal boundary layer height. These also have methane mixing ratios above the ~2,000 ppb (typical for 39°N in 2022). The mixing array is interpreted to reflect local mixing of microbially sourced methane into background air and a schematic mixing line is included on this diagram for illustrative purposes.

In this diagram, the isotopic composition of background tropospheric air (red circle) methane ($\delta^{13}C$ and δD values) is shifted from its source methane as a result of **KIE** (**kinetic isotope effects**[¶]—see *SI Appendix*) associated with sink reactions for methane (predominantly reaction with the $^{\bullet}OH$ radical, and to a lesser extent to sinks attributable to $Cl^{\bullet}$, $O(^1D)$, and soil oxidation reactions), and these KIE reflect different sink reaction rates for different isotopologues [c.f., (26–28)]. The KIE for $^{\bullet}OH + {}^{13}CH_4$ is only about 1.0039, but $^{\bullet}OH + {}^{12}CH_3D$ is much slower with a KIE of ~1.3. This leads to different lifetimes (e.g., ~30% longer for $^{12}CH_3D$ compared to CH_4) for the isotopologues in air (26). The effect for δD is more pronounced than for $\delta^{13}C$, and the difference in composition makes it possible to see, for instance, the effect of local contributions to atmospheric methane. Fig. 1*A* shows little change in $\delta^{13}C$ relative to δD. There have been relatively few measurements of the other rate constants [e.g., (27)] and we have to calculate (model) KIE for other isotopologues using electronic structure methods; because this approach yields high-precision frequency shifts, the precision on the relative rates (KIE) is better than the accuracy (absolute rate constants).

Data for doubly substituted isotopologues ($\Delta^{12}CH_2D_2$ and $\Delta^{13}CH_3D$—*SI Appendix*, Table S1) for the same samples are presented in Fig. 1*B*. A similar offset for the isotopic compositions of methane in tropospheric air compared to that of the sources is seen and reflects KIE that produces an enrichment in heavier isotopologues resulting from the lower rates of sink reactions involving isotopologues with progressively more heavy-isotope substitutions [e.g., (26–28)].

Evidence of mixing can also be seen with the doubly substituted isotopologues. Fig. 1*B* also includes a mixing grid for mixing of atmospheric methane with methane from sources with compositions like those produced by the two predominant microbial pathways that generate different isotopic signatures [(24)—See also *SI Appendix*, Fig. S1 for a different mixing grid with natural gas and microbial sources]. Mixing lines on this grid are curved because of the way that $\Delta^{12}CH_2D_2$ and $\Delta^{13}CH_3D$ are defined. Straight mixing lines are, however, seen on plots of $\delta^{12}CH_2D_2$ and $\delta^{13}CH_3D$ (*SI Appendix*, Fig. S2). Adding clumped isotopes to traditional isotopes and trace gas measurements will thus provide a way to significantly improve source identification and apportioning at local and regional levels. Prior to this result, there was no equivalent of the red circle (a prior measurement of air methane) for the doubly substituted isotopologues.

While identifying contributions from local sources is a valuable application of isotopologue data, we first focus on the utility of isotopologue data for studies of the nature of global CH_4 sources and changes in the global methane cycle (sources and sinks) over decadal timescales.

Implications of Tropospheric Methane Isotopologue Data for Understanding Global Fluxes. As noted above, different rates of atmospheric sink reactions for isotopologues (KIE) exert a significant control over the resulting isotopic composition of methane in air. Enrichments of $^{12}CH_2D_2$, $^{13}CH_3D$, and $^{12}CH_3D$, leading to more positive $\delta^{13}CH_3D$, and $\delta^{12}CH_2D_2$ values on a global scale (Fig. 1 and *SI Appendix*, Fig. S1) result from several different kinetic isotope effects. The combined role of KIE for the sinks with $^{\bullet}OH$ and $Cl^{\bullet}$ generates ~5‰ increases in $\delta^{13}C$, ~130‰ increases for δD and $\delta^{13}CH_3D$, and ~200‰ increases for $\delta^{12}CH_2D_2$ for tropospheric methane relative to its primary sources (26, 27). KIE also produces the observed positive $\Delta^{12}CH_2D_2$ and $\Delta^{13}CH_3D$ values (clumped: $\Delta>0$) of methane in ambient (tropospheric) air (26, 27).

A potential added element for these two reactions is that the KIE for the reaction with the $^{\bullet}OH$ radical leads to strong positive shifts for $\Delta^{12}CH_2D_2$ (enhanced clumping) but not for $\Delta^{13}CH_3D$ (26, 27). The reaction with $Cl^{\bullet}$ however generates greater effects for the ^{13}C-containing isotopologues [(8), (9), see also (11)]. This combination raises the possibility that $\Delta^{13}CH_3D$ might also provide information about changes in the proportional contribution of the $Cl^{\bullet}$ sink reaction.

Insight into Global Microbial Flux from Air Isotopologues. While the measurements of isotopologues in air have strongly positive $\Delta^{12}CH_2D_2$, like recent predictions (26–29) using forward, bottom–up isotopologue models, an important difference is revealed. The predictions overestimated the degree of clumping for both doubly substituted isotopologues, a feature that can be traced to assignments of the isotopologic mix of methane emitted from microbial methanogenic sources such as wetlands.

At the time these modeling studies [e.g., (26–29)] were undertaken, evidence existed that pure cultures of methanogens generate strongly anticlumped methane (negative $\Delta^{12}CH_2D_2$ and $\Delta^{13}CH_3D$ values); however, it was also known that pure culture experiments may not capture the true signature of methanic microbial communities in situ. When cellular-level metabolic rates are slow,

[¶]KIE = k_{12CH4}/k_i, where k_i is the rate constant of the isotopologue of interest at a specific temperature.

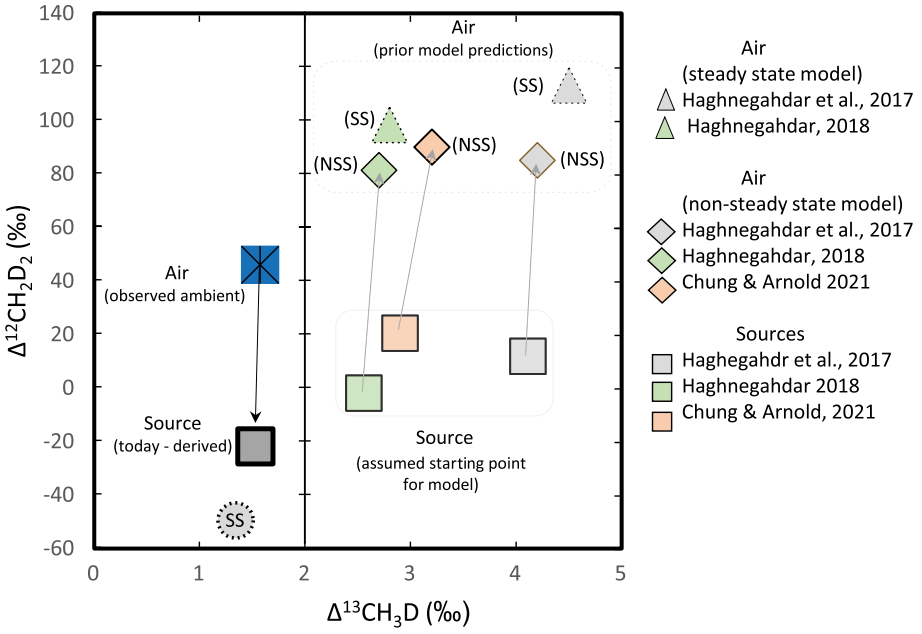

Fig. 2. Plot of $\Delta^{12}CH_2D_2$ vs. $\Delta^{13}CH_3D$ (‰) illustrating the fundamentally different structure and results of constraints imposed by modeling measurements of methane in tropospheric air versus predicting the composition from assumptions about sources. The vertical line separates the observed measurement and derived source composition which have lower $\Delta^{13}CH_3D$ values from the prior model predictions which started with a source composition having higher $\Delta^{13}CH_3D$ values. The square symbol (blue with star) is the composition of observed ambient air methane (today). The gray square symbol is the derived composition of the source flux (today). The stippled gray circle (labeled SS) is what would be attained if the atmosphere and sources were in steady state flux = sink flux) for an atmospheric methane composition like the one observed. On the right side of the plot, at higher $\Delta^{13}CH_3D$ are plotted the assumed composition for the source flux used by [(24)—green], [(27)—pink], [(28)—tan]. The diamond symbols are the derived (predicted) composition of air methane (same colors) and the stippled triangle symbols are the composition of air for the same sources when at steady state.

which is relevant in many natural environments, greater clumping is seen (30, 31). Furthermore, in nature, methanogens coexist with methanotrophs, microbes that consume (oxidize) methane produced by methanogens. Methanotrophs had been shown to shift isotopologues to more clumped (less negative) $\Delta^{12}CH_2D_2$ and $\Delta^{13}CH_3D$ values [(20, 29, 32, 33), but see refs. 34 and 35 for recent exceptions]. These two considerations led the modeling studies [e.g., (26–29)] to assign more clumped (less negative) $\Delta^{12}CH_2D_2$ and $\Delta^{13}CH_3D$ values than those seen in pure culture to the global microbial source flux(es). In turn, these models predicted strongly positive $\Delta^{12}CH_2D_2$ and $\Delta^{13}CH_3D$ values for air, more positive than our direct measurements (Fig. 2).

Using a box model (*SI Appendix*), we show here that the observed isotopologue composition of ambient tropospheric air requires a significantly less positive $\Delta^{12}CH_2D_2$ value (more anti-clumped) for the (total) source flux Fig. 2. This source flux has negative (anticlumped) $\Delta^{12}CH_2D_2$ indicating that the major microbial sources (e.g., wetlands, landfills, and agriculture)[#] have anticlumping, similar to gases collected in pure culture studies. The $\Delta^{13}CH_3D$ values are also lower, but not as low as those seen in pure culture studies. The reason for this less clumped source composition suggests that the most important pathways for methane emitted to the atmosphere are those where methanogenesis occurs at more rapid cellular rates and also that the signature is weighted toward methanogenesis because, in settings where methanotrophy dominates, emissions are lower.

The fact that the total source is fed by a combination of microbial contributions with strongly negative $\Delta^{12}CH_2D_2$ values and fossil fuel contributions with positive $\Delta^{12}CH_2D_2$ values amplifies the signal provided by $\Delta^{12}CH_2D_2$ values to track changes in their relative contributions. The smaller difference for $\Delta^{13}CH_3D$ values makes this tracer less sensitive to changes in microbial/fossil fuel flux ratios, but it may provide different constraints because the shifts generated by sink reactions with $^{\bullet}OH$ radicals are small compared to the larger shifts for the sink reaction with $Cl^{\bullet}$. Thus, it may be possible to use $\Delta^{13}CH_3D$ values to track variations in the $Cl^{\bullet}$ sink reactions, should the proportional loss to the $Cl^{\bullet}$ sink increase significantly above its present levels. Furthermore, some sources with similar $\Delta^{12}CH_2D_2$ have different $\Delta^{13}CH_3D$; for instance, those associated with microbially sourced methane compared to unequilibrated thermogenic methane (22), leading to the suggestions that on local scales, $\Delta^{13}CH_3D$ values may be a valuable asset for identifying which is most important.

Isotopologues Track Apportionment of Methane Fluxes on Decadal Timescales. The rise of atmospheric methane has been evaluated using bulk isotope measurements of atmospheric methane [e.g., (6–11, 13)]; however, the conclusions made in these studies differ; Rice (13) argues on the basis of time series δD measurements that fossil fuel sources were flat leading up to the plateau in methane concentration between 1999 and 2006 and only rose recently; whereas Milkov (10), Lan (11), and Basu (36) argue on the basis of $\delta^{13}C$ variations that recent enhancements in wetland emissions explain the most recent rise; other studies, Rigby (8), Turner (9), and Chung and Arnold (28) have argued that other factors related to the strength of sinks and KIE also could play a role in controlling the recent rise of atmospheric methane. As argued by Rigby (8), it would appear clear that additional constraints and data with models are needed to fully understand the controls in the rapidly changing understanding of global atmospheric methane in the past, present, and future.

Here, we use a box model to evaluate how much additional data from $\Delta^{12}CH_2D_2$ and $\Delta^{13}CH_3D$ may add to understanding the temporal trend in atmospheric methane, and specifically, whether they may differentiate the contributions of fossil fuel and

[#]It is conceivable, if for instance landfill and or wetland sources are found to have less anti-clumping and agricultural sources are found to have greater anticlumping, (or vice versa) that this analysis would point to one or the other as the primary reason for the observed compositions.

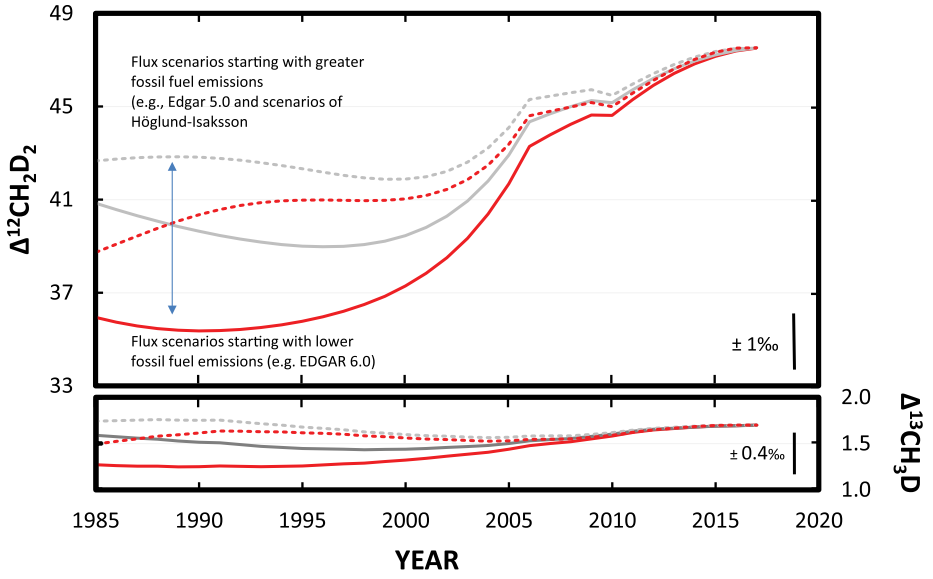

Fig. 3. Plot of model for variation of $\Delta^{12}CH_2D_2$ (*Top*) and $\Delta^{13}CH_3D$ (*Bottom*) scaled to have proportional signal compared to uncertainty (bars on the lower right of each plot. Four model scenarios are explored (see *SI Appendix* for more detail) using different parameterizations of sources, but the same parameterization for evolution of $\delta^{13}C$, δD, sink, and rise in concentration. Parameterizations are broadly matched to the EDGAR (Emissions Database for Global Atmospheric Research) versions 6.0 and 5.0 (35) with and without substitution of a smoothed version of the natural gas fluxes proposed by Höglund-Isaksson (38). The models are constrained to converge on the present-day composition for atmospheric methane and solved using an inverse approach. The models show that $\Delta^{12}CH_2D_2$ (*Top*) and $\Delta^{13}CH_3D$ (*Bottom*) vary in different ways for the different source flux parameterizations even when they reproduce the same evolution of $\delta^{13}C$, δD, sink, and rise in concentration. Solid red line is for fluxes broadly matched to EDGAR 6.0. Solid gray line is for fluxes broadly matched to EDGAR 5.0. Dashed lines are for fluxes that substitute the smoothed version of natural gas fluxes proposed by Höglund-Isaksson (38) into the EDGAR 6.0 (red dashed) and EDGAR 5.0 (gray dashed) fluxes.

microbial sources. **EDGAR** [**Emissions Database for Global Atmospheric Research** (37)] provides high-quality constraints on methane fluxes from major anthropogenic sources, and different versions of EDGAR reflect uncertainty in understanding of the apportionment of these fluxes over the past few decades. We used two versions of EDGAR and also considered another model of fossil fuel flux (38) to build four different scenarios for anthropogenic source fluxes for our box model. EDGAR does not include wetland emissions and those are calculated (a free variable) to close the flux balance needed by the model. Each scenario broadly follows one of four parameterizations[‖] of anthropogenic source fluxes to obtain an estimate of the composition and evolution of $\Delta^{12}CH_2D_2$ and $\Delta^{13}CH_3D$ through time (Fig. 3). The aim is to determine whether the isotopologue data would yield detectable signatures to distinguish among the four modeled scenarios.

The temporal model evolution of atmospheric methane for the different scenarios is generally similar in form, with lower values of $\Delta^{12}CH_2D_2$ and $\Delta^{13}CH_3D$ in the 1980's, followed by a rise in values starting in the 1990 s that levels off in the second decade of this century. This form is driven by the principles similar to those that drove the irregular rise of methane—the increase in $\Delta^{12}CH_2D_2$ and $\Delta^{13}CH_3D$ values is attributed to an approach to steady state as the rise tapered off.

As seen in Fig. 3, both $\Delta^{12}CH_2D_2$ and $\Delta^{13}CH_3D$ are sensitive to the chosen test case scenarios for anthropogenic CH_4 sources, and since these scenarios are broadly similar to those that have been proposed by EDGAR, and because other model parameters (sink, concentration history, bulk isotopes, and KIE) are kept constant (the same), it can be concluded that the isotopologue approach adds information and improves the ability to refine understanding of the global methane cycle. Reaching this goal will be a challenge not only because of the difficulty and time involved in making these measurements but also because of the scale of this global problem where methane and its isotopologues vary from pole to pole and on seasonal, annual, and decadal timescales (2, 3, 11–14, 36, 39–41). It will therefore be important that more laboratories develop the instrumentation and capability to extract and analyze the isotopologue composition of atmospheric methane. Measurement of air from the past will prove more challenging because existing sample archives are highly precious and only contain small amounts of air. Trapped air samples from natural settings, like arctic firn (partially compacted granular snow that persists from prior years) should provide a means to explore methane isotopologue changes in the past, but these may become increasingly rare as global warming melts these icy archives.

Digging further into the underlying reason for the variation of $\Delta^{12}CH_2D_2$ among the four investigated model anthropogenic source flux scenarios, we hypothesize that this is in large part due to the greater contrast between negative $\Delta^{12}CH_2D_2$ for global microbial sources compared to fossil fuel sources. A critical part of this model exercise and this response to source was that the derived composition of the total source would evolve differently, depending on whether fossil fuel or microbial wetland fluxes drove the rise in atmospheric methane concentration (*SI Appendix*, Fig. S12). Further to this point, the D/H required of the wetland source must change significantly if the rise is due to fossil sources but is stable if wetlands control the rise, which would lend support to recent findings that attribute the rise to increases in wetland fluxes on the basis of bulk ^{13}C abundances [(8, 10, 14, 31) but see ref. 40] for arguments that the ^{13}C abundances permit alternate interpretations).

Conclusions

This study contributes three findings relating isotopologue data to atmospheric methane cycling. Isotopologue measurements of atmospheric methane provide additional, independent constraints

[‖]The parameterization of anthropogenic fluxes is described in more detail in *SI Appendix* and includes the following: one scenario broadly matches fluxes of EDGAR 6.0 (37), but smoothed to reduce artifacts of short term change; another broadly matches fluxes of EDGAR 5.0 (37), also smoothed; a third substitutes a smoothed version of natural gas fluxes proposed by Höglund-Isaksson (38) into the EDGAR 6.0 scenario; and the fourth substitutes a smoothed version of natural gas fluxes proposed by Höglund-Isaksson (38) into EDGAR 5.0 scenario.

on contributions from local sources that promise to strengthen source apportionment at regional and local levels. At a global level, the measurements of atmospheric methane isotopologues show that microbial CH_4 sources have clearly distinct (negative) $\Delta^{12}CH_2D_2$ values compared to fossil fuel sources, and this makes atmospheric methane isotopologue measurements more sensitive for source apportionment than previously suggested. In contrast, $\Delta^{13}CH_3D$ variations appear to be less sensitive for source apportionment, except in local source apportionment efforts where sources have distinctly different $\Delta^{13}CH_3D$. Finally, a model analysis shows that $\Delta^{12}CH_2D_2$ data and $\Delta^{13}CH_3D$ data will add to understanding of decadal changes in the global methane cycle (past and future), specifically as it relates to fluxes from fossil fuel and microbial contributions to global methane burden.

Materials and Methods

Sampling. Surface air, chamber, and smoke samples were collected into Tedlar bags (10, 20, or 200 L) using a Gast (P704) diaphragm pump. Methane from anaerobic incubations was extracted from the headspace using an air-tight syringe with a valve. Methane from bubbles released from a rice paddy was collected in a funnel and then into a 50-cc syringe with a valve.

For air samples, we generally use 600 to 800 L of sample, but we have worked with some samples as small as 200–400 L. For chamber and smoke samples, methane concentrations were higher and smaller samples were used. Sample size was determined to provide approximately 1.5 to 6 cc of purified methane, which was necessary for the low abundance isotopologue abundance measurements. For CO_2-rich samples, CO_2 and water were removed using a liquid nitrogen-cooled trap before introduction to the purification manifold.

Preconcentration and Purification. At the entrance to the purification manifold, the gas passes through a 400 cc canister trap filled with dehydrated silica gel (preheated to 150 °C overnight). The sample is then passed through a set of liquid nitrogen-cooled U-traps [6 in total, ½ inch OD, ~40 cm length, packed with 100–120 mesh particle size HayeSep DB porous polymer (Sigma-Aldrich®)] by pumping with a mechanical vacuum pump on the far end of the manifold. The restriction of the canister trap holds the gas pressure before the set of HayeSep DB traps at ~200 mbar, thus allowing a 600 L sample to pass through in about 2 h. Once the sample has been completely pumped through this canister trap, the upstream valve is closed, and the sample is pumped until the baseline stabilizes.

Following this, the sample is warmed to ~150 °C to transfer it to a second (smaller) liquid nitrogen-cooled HayeSep DB filled trap (3/8″ od, ~40 cm length), again, by pumping on the downstream side. For syringe samples, the samples are transferred directly to this second U trap because the concentration of balance gases (nitrogen and oxygen) is low. Once the transfer is complete and the pressure has dropped to about 10 mbar, this trap is warmed to ~−117 °C using an ethanol slush to release most of the nitrogen, some oxygen, and possibly some krypton, but to retain the methane.

After 30 min, the trap is isolated and the preconcentrated sample is transferred using a sample tube with silica gel (freezing onto the silica gel by cooling with liquid nitrogen) to a purification manifold that is very similar in design to the manifold used at UCLA (16). The sample is transferred to an injection loop filled with liquid nitrogen-cooled silica gel, which is subsequently warmed and injected using a 2-way Valco switching valve into an SRI 310C gas chromatograph. The chromatographic column is 1/8″ diameter and 25′ long filled with 5 Å mol sieve held at 54 °C. The helium carrier gas flow of 35 mL/min separates methane from krypton, nitrogen, and oxygen. A thermal conductivity detector is used to identify the start and end of the CH_4 peak, and the flow is manually diverted into a liquid nitrogen-cooled collection loop filled with silica gel through this interval. Additional details and schematics of our extraction and purification manifold can be found in *SI Appendix*, Figs. S18 and S19).

Once the sample is collected, the collection loop contains methane and helium and it is necessary to remove the carrier gas without loss of methane. At UCLA, this is done by slowly pumping the helium away. At UMD, we use a slightly different strategy by pumping through a second U trap (filled with silica gel) to trap any methane that might be drawn away as the helium is outgassed. Once the helium is quantitatively removed, the remaining methane is transferred to this second loop, which is then warmed and transferred to a sample tube filled with silica gel after the recovered yield is measured manometrically.

Measurements. The purified methane samples were then analyzed using the Panorama high-resolution mass spectrometer (Nu Instrument) at UMD. Ion currents of $^{12}CH_4^+$, $^{13}CH_4^+$, $^{12}CH_3D^+$, $^{13}CH_3D^+$, and $^{12}CH_2D_2^+$ were measured using a minimum mass resolving power (MRP) of 36,000 (5%–95%) for clean separation of $^{12}CH_2D_2$ from $^{13}CH_3D$, corresponding to an approximate entrance slit width of 35 μm (16). Methane was measured using sample standard bracketing relative to a working gas (UMD-1). We see a minor dependence of isotopic composition on the pressure balance between the sample and reference that we hypothesize is related to production of both CH_3^+ and CH_4^+ in the source. We postprocess the data to determine the intercept where sample and working gas pressures are equal. We also remove the first cycle from each set of sample standard bracketing pairs and any 3 σ outliers during each analytical session, which last between 24 and 36 h. Precisions of the mass spectrometric measurements based on internal reproducibility (counting statistics for rare isotopologues) are reported in *SI Appendix*, Table S1.

Data are reported in standard notation (definitions and description in *SI Appendix*). Calibrations reported here are done against AL-1 from MIT and the clumped isotopologues are calibrated by comparison with three thermal equilibrations using γ-alumina catalyst (20). We tested our reproducibility of samples with different $\Delta^{12}CH_2D_2$ and $\Delta^{13}CH_3D$ by sharing composite samples of methane separated from atmospheric air, methane from wetlands, and our reference gas with the California Institute of Technology, and by comparison of analyses of large methane samples provided for two other gases previously measured by MIT (17, 18) and UCLA (16) (*SI Appendix*, Tables S2 and S3).

Data, Materials, and Software Availability. Model calculations data have been deposited in Digital Repository for the University of Maryland (DRUM) at http://hdl.handle.net/1903/31091 (42).

ACKNOWLEDGMENTS. Funding for the UMD Panorama mass spectrometer has come from U.S. NSF [NSF MRI EAR-1725766 MRI: Acquisition of a High Mass Resolution/High Sensitivity Isotope Ratio Mass Spectrometer for Earth Sciences 2017–2020 (J.F., A.J.K., R.R.D.)] as well as infrastructure support for the facility from the Geology Department, the College of Computer, Mathematics, and Natural Sciences, and the Provost's Office at UMD. Funding for the establishment of protocols for air sampling was provided by Water Resources Research Act Program Annual Base grant US Department of the Interior–US Geological Survey 2020, 2021 (J.F. and M.A.H.). Funding to support M.A.H. was provided by a UMD President's Postdoctoral Fellowship Program for providing funding that aided in supporting this work, and then by U.S. NSF grant (EAR-PF: 2052834) (M.A.H.). Finally, we thank Doug Rumble for providing samples of natural gas and for assistance during the commissioning of our mass spectrometer.

Author affiliations: [a]Department of Geology, University of Maryland, College Park, MD 20742; [b]Earth System Science Interdisciplinary Center, University of Maryland, College Park, MD 20742; [c]Smithsonian Environmental Research Center, Edgewater, MD 21037; [d]Department of Environmental Science and Technology, University of Maryland, College Park, MD 20742; [e]Division of Geological and Planetary Sciences, California Institute of Technology, Pasadena, CA 91125; [f]Department of Earth, Atmospheric and Planetary Sciences, Massachusetts Institute of Technology, Cambridge, MA 02139; and [g]Department of Oceanic and Atmospheric Science, University of Maryland, College Park, MD 20742

Author contributions: M.A.H., A.B., and J.F. designed research; M.A.H., J.S., N.H., N.D.H., N.K., S.A.Y., A.J.K., A.B., and J.F. performed research; M.A.H., J.E., S.O., A.B., C.M., and J.F. contributed new reagents/analytic tools; M.A.H., R.R.D., and J.F. analyzed data; M.A.H. investigation, project administration, methodology, review and editing; J.S. methodology and investigation; N.H. methodology; J.S., N.D.H., S.A.Y., R.R.D., and C.M. review and editing; J.E. and S.O. investigation review and editing; J.F. investigation, project administration, methodology, review and editing; and M.A.H. and J.F. wrote the paper.

1. E. J. Dlugokencky, E. G. Nisbet, R. Fisher, D. Lowry, Global atmospheric methane: Budget, changes and dangers. *Philos. Trans. R. Soc. A: Math., Phys. Eng. Sci.* **369**, 2058–2072 (2011).
2. X. Lan, K. W. Thoning, E. J. Dlugokencky, Trends in globally-averaged CH_4, N_2O, and SF_6 determined from NOAA Global Monitoring Laboratory measurements. Version 2023-04. https://doi.org/10.15138/P8XG-AA10.
3. E. G. Nisbet *et al.*, Very strong atmospheric methane growth in the 4 years 2014–2017: Implications for the Paris Agreement. *Global Biogeochem. Cycles* **33**, 318–342 (2019).
4. E. Nisbet, A. Jones, J. Pyle, U. Skiba, Rising methane: Is there a methane emergency? *Philos. Trans. R. Soc. A* **380**, 20210334 (2022).
5. M. Saunois *et al.*, The global methane budget 2000–2017. *Earth Syst. Sci. Data* **12**, 1561–1623 (2020).

6. E. G. Nisbet *et al.*, Atmospheric methane: Comparison between methane's record in 2006–2022 and during glacial terminations. *Global Biogeochem. Cycles* **37**, e2023GB007875 (2023).
7. H. Schaefer *et al.*, A 21st-century shift from fossil-fuel to biogenic methane emissions indicated by $^{13}CH_4$. *Science* **352**, 80–84 (2016).
8. M. Rigby *et al.*, Role of atmospheric oxidation in recent methane growth. *Proc. Natl. Acad. Sci. U.S.A.* **114**, 5373–5377 (2017).
9. A. J. Turner, C. Frankenberg, P. O. Wennberg, D. J. Jacob, Ambiguity in the causes for decadal trends in atmospheric methane and hydroxyl. *Proc. Natl. Acad. Sci. U.S.A.* **114**, 5367–5372 (2017).
10. A. Milkov, S. Schwietzke, G. Allen, O. Sherwood, G. Etiope, Using global isotopic data to constrain the role of shale gas production in recent increases in atmospheric methane. *Nat. Sci. Rep.* **10**, 4199 (2020).
11. X. Lan *et al.*, Improved constraints on global methane emissions and sinks using $\delta^{13}C\text{-}CH_4$. *Global Biogeochem. Cycles* **35**, e2021GB007000 (2021).
12. P. Bousquet *et al.*, Contribution of anthropogenic and natural sources to atmospheric methane variability. *Nature* **443**, 439–443 (2006).
13. A. L. Rice *et al.*, Atmospheric methane isotopic record favors fossil sources flat in 1980s and 1990s with recent increase. *Proc. Natl. Acad. Sci. U.S.A.* **113**, 10791–10796 (2016).
14. R. Fujita *et al.*, Global and regional CH_4 emissions for 1995–2013 derived from atmospheric CH_4, $\delta^{13}C\text{-}CH_4$, and $\delta D\text{-}CH_4$ observations and a chemical transport model. *J. Geophys. Res.: Atmos.* **125**, e2020JD032903 (2020).
15. J. M. Eiler *et al.*, A high-resolution gas-source isotope ratio mass spectrometer. *Int. J. Mass Spectrom.* **335**, 45–56 (2013).
16. E. D. Young, D. Rumble III, P. Freedman, M. Mills, A large-radius high-mass-resolution multiple-collector isotope ratio mass spectrometer for analysis of rare isotopologues of O_2, N_2, CH_4 and other gases. *Int. J. Mass Spectrom.* **401**, 1–10 (2016).
17. S. Ono *et al.*, Measurement of a doubly substituted methane isotopologue, $^{13}CH_3D$, by tunable infrared laser direct absorption spectroscopy. *Anal. Chem.* **86**, 6487–6494 (2014).
18. Y. Gonzalez *et al.*, Precise measurements of $^{12}CH_2D_2$ by tunable infrared laser direct absorption spectroscopy. *Anal. Chem.* **91**, 14967–14974 (2019).
19. D. Stolper *et al.*, Formation temperatures of thermogenic and biogenic methane. *Science* **344**, 1500–1503 (2014).
20. D. T. Wang *et al.*, Nonequilibrium clumped isotope signals in microbial methane. *Science* **348**, 428–431 (2015).
21. E. D. Young *et al.*, The relative abundances of resolved $^{12}CH_2D_2$ and $^{13}CH_3D$ and mechanisms controlling isotopic bond ordering in abiotic and biotic methane gases. *Geochim. Cosmochim. Acta* **203**, 235–264 (2017).
22. G. Dong *et al.*, Clumped isotope effects of thermogenic methane formation: Insights from pyrolysis of hydrocarbons. *Geochim. Cosmochim. Acta* **303**, 159–183 (2021).
23. P. M. Douglas *et al.*, Methane clumped isotopes: Progress and potential for a new isotopic tracer. *Org. Geochem.* **113**, 262–282 (2017).
24. M. J. Whiticar, "The biogeochemical methane cycle" in *Hydrocarbons, Oils and Lipids: Diversity, Origin, Chemistry and Fate* (Springer, 2020), pp. 669–746.
25. D. L. Eldridge *et al.*, Comparison of experimental vs theoretical abundances of $^{13}CH_3D$ and $^{12}CH_2D_2$ for Isotopically equilibrated systems from 1 to 500 C. *ACS Earth Space Chem.* **3**, 2747–2764 (2019).
26. M. A. Haghnegahdar, E. A. Schauble, E. D. Young, A model for $^{12}CH_2D_2$ and $^{13}CH_3D$ as complementary tracers for the budget of atmospheric CH_4. *Global Biogeochem. Cycles* **31**, 1387–1407 (2017).
27. A. R. Whitehill *et al.*, Clumped isotope effects during OH and Cl oxidation of methane. *Geochim. Cosmochim. Acta* **196**, 307–325 (2017).
28. E. Chung, T. Arnold, Potential of clumped isotopes in constraining the global atmospheric methane budget. *Global Biogeochem. Cycles* **35**, e2020GB006883 (2021).
29. M. Haghnegahdar, *Theoretical Study of Tellurium Isotope Fractionations in Ore-forming Systems, and Studies of Doubly Substituted Isotopologues of Methane* (UCLA, 2018).
30. J. J. Jautzy, P. M. Douglas, H. Xie, J. M. Eiler, I. D. Clark, CH_4 isotopic ordering records ultra-slow hydrocarbon biodegradation in the deep subsurface. *Earth Planet. Sci. Lett.* **562**, 116841 (2021).
31. Q. Gropp, I. Halevy. Jin, Controls on the isotopic composition of microbial methane. *Sci. Adv.* **8**, eabm5713 (2022).
32. S. Ono *et al.*, Clumped isotopologue fractionation by microbial cultures performing the anaerobic oxidation of methane. *Geochim. Cosmochim. Acta* **293**, 70–85 (2021).
33. J. L. Ash *et al.*, Exchange catalysis during anaerobic methanotrophy revealed by $^{12}CH_2D_2$ and $^{13}CH_3D$ in methane. *Geochem. Perspect. Lett.* **10**, 26–30 (2019).
34. T. Giunta *et al.*, Extreme methane clumped isotopologue bio-signatures of aerobic and anaerobic methanotrophy: Insights from the Lake Pavin and the Black Sea sediments. *Geochim. Cosmochim. Acta* **338**, 34–53 (2022).
35. S. J. Krause, J. Liu, E. D. Young, T. Treude, $\Delta^{13}CH_3D$ and $\Delta^{12}CH_2D_2$ signatures of methane aerobically oxidized by *Methylosinus trichosporium* with implications for deciphering the provenance of methane gases. *Earth Planet. Sci. Lett.* **593**, 117681 (2022).
36. S. Basu *et al.*, Estimating emissions of methane consistent with atmospheric measurements of methane and $\delta^{13}C$ of methane. *Atmos. Chem. Phys.* **22**, 15351–15377 (2022).
37. M. Crippa *et al.*, High resolution temporal profiles in the Emissions Database for Global Atmospheric Research. *Sci. Data* **7**, 121 (2020).
38. L. Höglund-Isaksson, Bottom-up simulations of methane and ethane emissions from global oil and gas systems 1980 to 2012. *Environ. Res. Lett.* **12**, 024007 (2017).
39. P. Quay *et al.*, The isotopic composition of atmospheric methane. *Global Biogeochem. Cycles* **13**, 445–461 (1999).
40. Z. Zhang *et al.*, Anthropogenic emission is the main contributor to the rise of atmospheric methane during 1993–2017. *Natl. Sci. Rev.* **9**, nwab200 (2022).
41. Z. Zhang *et al.*, Recent intensification of wetland methane feedback. *Nat. Clim. Change* **13**, 430–433 (2023).
42. M. A. Haghnegahdar *et al.*, Tracing sources of atmospheric methane using clumped isotopes. Digital Repository at the University of Maryland (DRUM). http://hdl.handle.net/1903/31091. Deposited 23 October 2023.